Rare Metal Materials and Engineering
Volume 55, Issue 12, December 2026
Available online at www.rmme.ac.cn

Science Press

Cite this article as: Zhou Baocheng, Huang Qianqian, Liu Shiwei, et al. Effect of Scratching Speed on Nano-scratched Performance of γ-TiAl Alloy Under Water Lubrication[J]. Rare Metal Materials and Engineering, 2026, 55(12): 3053-3066. DOI: https://doi.org/10.12442/j.issn.1002-185X.20250648.

ARTICLE

Effect of Scratching Speed on Nano-scratched Performance of γ-TiAl Alloy Under Water Lubrication

Zhou Baocheng[1,2], Huang Qianqian[1], Liu Shiwei[1], Cao Hui[1,3], Rui Zhiyuan[1,3], Feng Ruicheng[1,3]

[1] School of Mechanical and Electrical Engineering, Lanzhou University of Technology, Lanzhou 730050, China; [2] Green Aviation Technology Research Institute, Chongqing Jiaotong University, Chongqing 401135, China; [3] Engineering Research Center for New Equipment of Nonferrous Metallurgy, Ministry of Education, Lanzhou University of Technology, Lanzhou 730050, China

Abstract: γ-TiAl alloys feature superior high-temperature performance and low-density properties. However, the inherent brittleness of γ-TiAl alloys poses significant challenges to precision machining. As a highly promising machining approach, water lubrication enables temperature reduction and mitigates frictional heat accumulation, tool wear, and crack-associated defects. This work investigated the effects of nano-scratching speed on scratching force, temperature evolution, plastic deformation, and surface quality of single-crystal γ-TiAl alloy under water lubrication. The results show that the coupling effect between scratching speed and water lubrication governs the machinability and surface quality of single-crystal γ-TiAl alloys. An increase in scratching speed substantially elevates scratching force and frictional heat, which further induces local temperature rise and stress concentration. In comparison, a 1-nm-thick water lubrication layer yields minor temperature fluctuation of the substrate and delivers favorable cooling capacity. At a scratching speed of 400 m/s, water lubrication alleviates surface plastic deformation and damage, promotes chip accumulation, and reduces surface roughness. Experimental observations further confirm that scratching speed exerts a pronounced effect on surface quality.

Key words: γ-TiAl alloy; nano-scratching; scratching speed; water lubrication; surface quality

1 Introduction

In recent years, with the increasing demand for high-performance materials in the aerospace industry, the research and development of high-temperature structural materials has become a key direction in material science[1]. However, their complex processing characteristics have posed significant challenges to practical application. The high strength of γ-TiAl alloy requires greater force during processing. However, due to its low thermal conductivity, heat cannot be dissipated effectively, resulting in a rapid temperature rise in the processing area. In addition, the strong interaction between the γ-TiAl alloy and the tool, combined with the high work hardening rate, produces significant local deformation heat, which further increases the processing difficulty[2]. The combined effect of these factors not only leads to the temperature rise during machining, but also induces significant thermal effects on the machined surface. This results in surface or subsurface micro-damage and even crack formation[3], which restricts the wide application of γ-TiAl alloy in high-performance structural components. As a common lubrication method, water lubrication can effectively reduce friction and wear, thereby improving the processing quality[4–5]. In the context of green and sustainable manufacturing, the appropriate selection and use of lubricants can effectively reduce energy consumption, improve product quality, be beneficial to health and safety environment, and optimize the overall performance of mechanical systems[6].

Received date: December 25, 2025
Foundation item: National Natural Science Foundation of China (52365018); Natural Science Foundation of Gansu (25JRRA060, 24JRRA175); Hongliu Outstanding Youth Foundation of Lanzhou University of Technology
Corresponding author: Rui Zhiyuan, Ph. D., Professor, School of Mechanical and Electrical Engineering, Lanzhou University of Technology, Lanzhou 730050, P. R. China, E-mail: zhiy_rui@163.com; Cao Hui, Ph. D., Associate Professor, School of Mechanical and Electrical Engineering, Lanzhou University of Technology, Lanzhou 730050, P. R. China, E-mail: caoh@lut.edu.cn

Copyright © 2026, Northwest Institute for Nonferrous Metal Research. Published by Science Press. All rights reserved.

Water is the most common lubricant in mechanical grinding and chemical mechanical polishing[7]. The addition of liquid can block the direct contact between the tool and the substrate, reduce the friction coefficient, and improve the surface quality after processing[8]. The resulting wet environment further optimizes the processing effect and reduces surface damage by changing the surface removal mechanism and lowering friction during nano-scratching. Shi et al[9] studied the surface removal process of copper film in an ultra-thin water environment by molecular dynamics (MD) simulation, and found that the interaction between water molecules and copper surface can significantly change the surface removal mechanism, reduce friction and thermal effects, and improve the surface removal efficiency and surface quality. Sharma et al[10] investigated the material removal and wear behavior of copper film in air and a wet environment using nanoindentation. They found that both the wear rate and material removal rate of copper film in wet environment were significantly lower than those in air, which was attributed to the reduction of friction and surface damage by water lubrication. Tian et al[11] studied the sliding friction behavior of water film on a copper/silver double-layer film at nanometer scale, and found that water film played a lubricating role between the copper/silver double-layer surfaces, which significantly reduced the friction force and improved the friction performance.

Zhou et al[12–13] studied the effects of water film and scratch load on tribological properties by MD simulation. They found that water film can reduce the friction coefficient and enhance heat dissipation during scratching. Wang et al[14] performed MD simulation to reveal the chemical mechanical polishing mechanism of Invar alloy under water lubrication condition. Their results show that appropriate water layer thickness and polishing speed can significantly reduce surface roughness and subsurface defects of the workpiece. Water lubrication significantly lowers the friction coefficient and improves the surface quality by blocking direct contact between the tool and the substrate during nano-scratching. The ultra-thin water layer and wet environment further optimize the processing effect and reduce surface damage by changing the surface removal mechanism and reducing the friction force. These studies demonstrate that thin water layer lubrication has important application value in nano-machining, which can effectively improve the machining performance and reduce tool wear.

During nano-scratching, the scratching speed significantly affects the material removal mechanism, surface quality and deformation-layer depth. Higher speed improves the processing efficiency but also increases surface damage and subsurface defects. Shikimaka et al[15] discussed the effects of scratching speed, load, and indenter direction on the deformation mechanism of silicon materials. They found that higher load and lower scratching speed led to more severe plastic deformation and surface damage. Zhu et al[16] investigated the effects of scratching direction and speed on friction and surface deformation during nano-scratching of single-crystal copper, and concluded that appropriate scratching direction and speed can optimize processing quality. Li et al[17] examined the plastic deformation mechanism of nano-copper at different scratching rates, and found that the dislocation motion was more complex at higher scratching rates, resulting in higher friction and material removal rate. Zhang et al[18] studied the effect of scratching speed on material removal rate and shear force via MD simulation, and found that increasing scratching speed reduced the material removal rate while elevating the local temperature. With the deepening of the research, the MD simulation of nano-machining process is gradually extended to the influence factors of surface quality and subsurface damage. Wang et al[19] established a prediction model for the critical cutting speed of ultra-high speed cutting based on the theory of stress wave propagation. They verified this model through experiments on 7050-T7451 aluminum alloy, which showed that the aluminum alloy underwent a ductile-brittle transition at a cutting speed above 5000 m/min, resulting in fragmented chips and brittle cracks on the chip surface. Su et al[20] performed orthogonal cutting experiments of high-strength alloy steel AerMet100. They found that with the increase in cutting speed, the serrated chips changed from a continuous strip at the macroscale to separate segments. The serrated chips produce microwaves on the machined surface, thereby increasing the surface roughness. Shimada et al[21] confirmed that faster cutting speed has less effect on surface roughness and deformation-layer depth.

The above research shows that during nano-scratching on metal surfaces, the selection of process parameters plays a vital role in the processing results, which directly affects the processing efficiency, surface quality, fatigue life, and tool wear. Increasing the scratching speed to enhance the processing efficiency often leads to aggravated surface damage and subsurface defects, which ultimately affect the quality and performance of the workpiece.

2 Simulation Method

2.1 Establishment of model

To study the effect of scratching speed on the nano-scratching process of γ-TiAl alloy under water lubrication, a water film with a thickness of 1 nm and a density of 1 g/cm^3 was employed in the model. The time step of the integral calculation was 0.001 ps. In nano-scratching, there are two main stages: relaxation and processing. During the relaxation stage, the model was equilibrated under the NVT ensemble at 300 K using a Nosé -Hoover thermostat for 30 ps. After relaxation, the system energy and pressure stabilized. In the production phase, the system was observed, and data were collected. To avoid introducing external interference during the observation process, the NVE ensemble is typically employed. However, the total momentum of the system changes due to the movement of the tool. Yet the NVE ensemble can ensure the realistic physical behavior of the core deformation zone, and it is therefore unnecessary to adopt velocity resetting or other methods to maintain the conservation of overall momentum of the system. The

machining process includes moving the tool at a constant speed and pressing it into the workpiece, and then scratching at a constant speed. In this research, the temperature of the water film was controlled at 300 K to simulate the heat dissipation process of water. Large-scale atomic/molecular massively parallel simulator (LAMMPS) was used for simulation[22]. Visualization was achieved using the open visualization tool (OVITO)[23]. Through the observations after processing, it can be seen that during processing, the equilibrium state of the workpiece itself is destroyed, the strain energy accumulation is distorted, and the atoms are squeezed. Fig. 1 shows the basic MD model used in the simulation, which consists of γ-TiAl alloy workpiece, diamond tool, and water layer. The cell structure of γ-TiAl alloy is similar to that of face-centered cubic (fcc) alloy, with $L1_0$-type face-centered tetragonal (FCT) crystal structure, which is beneficial to the improvement of stability and mechanical properties of the alloy. According to Ref. [24], the lattice constants a=b=0.4001 nm and c=0.4181 nm of the single-crystal γ-TiAl alloy were constructed. Given its diamond lattice structure and superior hardness relative to that of the γ-TiAl alloy workpiece, the diamond tool was modeled as a rigid body in the simulation. The workpiece has a boundary layer to prevent the overall rigid motion of the workpiece during nano-scratching. A thermostat layer was set above the boundary layer, which was regulated by the NVT ensemble with a damping coefficient of 0.1 to simulate the energy dissipation during atomic motion. To account for the distinct properties of nanomaterials compared with those of bulk metals, periodic boundary conditions were applied along the x and y axes, while the z-axis employed fixed boundary conditions to mitigate nanoscale nonlinear effects. For the water film, a vacuum layer was established in the z-direction (perpendicular to the workpiece surface) to prevent periodic image interactions. In the simulation, several atomic layers at the bottom of the workpiece were fixed, and thus the entire workpiece exhibited no drift velocity. The remaining model parameters of this study for the γ-TiAl alloy are shown in Table 1. Meanwhile, the force F_x and temperature T are calculated via LAMMPS using the following formulas.

$$T = \frac{Eq_{\mathrm{eV}}}{1.5k_{\mathrm{B}}} \tag{1}$$

where T is the local atomic temperature in K, E denotes the kinetic energy of target atom in eV, q_{eV} represents the conversion coefficient between electron volts and joules, and k_{B} is the Boltzmann constant.

$$F_x = 1000 \times \frac{F_{\mathrm{tool},x}}{N_{\mathrm{tool}}} \tag{2}$$

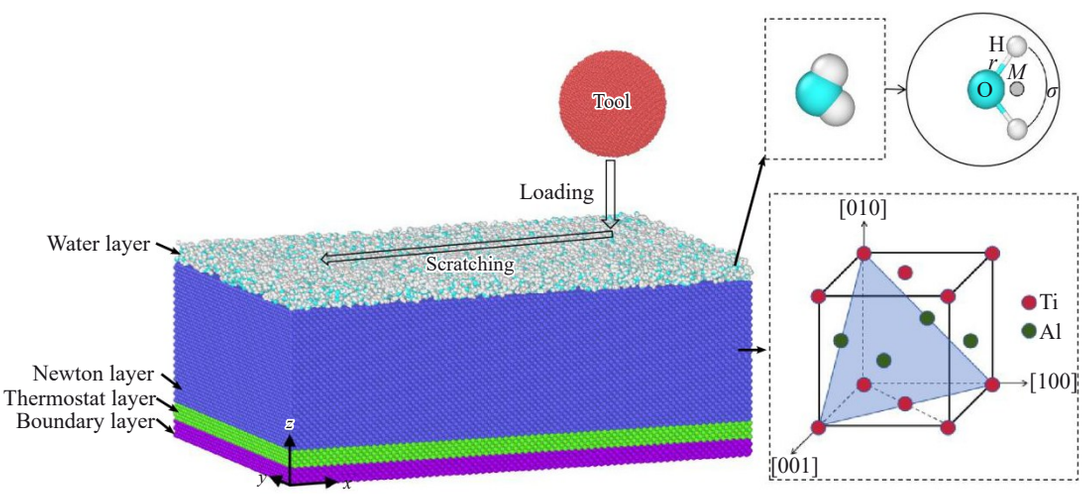


Fig.1 MD model for nano-scratching simulation of single-crystal γ-TiAl alloy

F_x is the average scratching force acting on the tool along the x direction in mN, $F_{\mathrm{tool},x}$ is the total force of all tool atoms in the x direction in N, N_{tool} stands for the number of interacting tool atoms, and the coefficient of 1000 corresponds to the unit conversion factor from Newton to millinewton.

2.2 Water molecule model and potential function

In MD simulations, the selection of potential functions directly affects the accuracy of the simulation results. The MD model constructed in this study consists of three parts: workpiece, tool, and water medium, involving five types of atoms (Ti, Al, C, H, and O). It is necessary to select appropriate potential functions to describe the interactions between various atoms to ensure simulation accuracy. The embedded atom method (EAM)[25–26] potential can accurately

Table 1 Model parameters of γ-TiAl alloy workpiece

Parameter	Value
Tool material	Diamond
Workpiece size	28 nm×18 nm×10 nm
Tool shape	Spherical with a radius of 3 nm
Potential energy function	EAM, Morse, and L-J
Number of atoms	324368
Timestep/ps	0.001
Scratching speed/m·s^{-1}	50, 100, 200, 400, 500
Water layer thickness/nm	1
Indentation depth/nm	2
Scratching distance/nm	15

describe the interactions between metal atoms. Therefore, the EAM potential function is used in this simulation to characterize the interactions between Ti and Al atoms, and its atomic energy expression is as follows:

$$E = \sum_i F_i(\rho_i) + \frac{1}{2}\sum_{j\neq i}\phi_{ij}(r_{ij}) \quad (3)$$

In the formula, F_i is the electron cloud density; ρ_i represents the embedding energy function; ϕ_{ij} is the potential interaction function between atoms i and j; r_{ij} denotes the distance between atoms i and j.

The Morse potential function is a typical potential function based on diatomic theory, which has been widely used in MD studies related to nanocutting of γ-TiAl alloys[27]. In this simulation, the Morse potential function is used to describe the interactions between workpiece atoms and tool atoms. Its expression is as follows:

$$u(r_{ij}) = D\left\{\exp\left[-2\alpha(r_{ij}-r_0)\right] - 2\exp\left[-2\alpha(r_{ij}-r_0)\right]\right\} \quad (4)$$

In the formula, D represents the bonding coefficient; α represents the potential energy gradient coefficient; r_0 represents the equilibrium distance between Ti-C and Al-C atoms. The reference values of each parameter are shown in Table 2.

The Lennard-Jones (L-J) potential function[28] is an empirical potential function suitable for simulating the interactions between two electrically neutral particles. In this simulation, the L-J potential function is used to calculate the interactions between water molecules and other atoms, and the wettability of water, the workpiece, and the workpiece surface is characterized by the L-J potential function. The L-J potential parameters between different atoms are shown in Table 3. Its expression is as follows:

$$V_{ij} = 4\varepsilon\left[\left(\frac{\sigma}{r}\right)^{12} - \left(\frac{\sigma}{r}\right)^{6}\right] \quad (5)$$

In the formula, V_{ij} represents the potential energy between atoms i and j; ε denotes the depth of the potential well, indicating the strength of attraction between reactive atoms; σ is the equilibrium distance between atoms at the minimum of the interaction potential; r is the distance between atoms.

The potential functions between different atoms are shown in Table 4.

There are various types of water molecule models, among which the TIP4P/Ew model has high consistency between its dynamic properties and experimental data[29]. This model can accurately simulate the diffusion coefficient, viscosity, dynamic structure factor, vibrational spectrum, and Raman spectrum of water molecules. Its core advantage lies in fully considering the intramolecular polarity and the formation of hydrogen bonds, which can truly reflect the movement behavior, spatial correlation, and dynamic correlation of water molecules. Based on the above advantages, the TIP4P/Ew model was adopted in this study to construct the water layer.

Table 2 Morse potential parameters of Ti-C and Al-C

Parameter	r_0/nm	α/nm^{-1}	D/eV
Al-C	0.220	27.8	0.28
Ti-C	0.1892	22.83	0.982

3 Results and Analysis

3.1 Effect of scratching speed on characterization force

To analyze the material deformation mechanism in the processing of single-crystal γ-TiAl alloy, it is necessary to obtain the force on the tool during scratching and connect the scratching force with the deformation behavior. The variation curves of the force and the scratching distance of the tool are shown in Fig.2.

Fig. 2 shows that during scratching simulation, scratching speed has a certain effect on the scratching force. At the beginning of scratching, the tangential force F_x first rises and gradually increases to a stable state, and fluctuates near the stable value. The main reason for the fluctuation of tangential force is the occurrence and evolution of dislocation defects in single-crystal γ-TiAl alloy. In the early stage of scratching, the increase in scratching force becomes more pronounced at faster scratching speed, i. e., the slope of F_x curve becomes larger. This is because the faster scratching speed leads to stronger friction and greater scratching heat during scratching. Faster scratching speed accelerates the deformation rate of the workpiece in the contact area, significantly enhancing the material hardening effect. Consequently, the scratching force increases.

Table 3 L-J interatomic potential parameters

Parameter	Ti-O	Ti-H	Al-O	Al-H	C-O	C-H	O-O	O-H	H-H
σ/nm	0.27769	0.29339	0.28787	0.12965	0.36	0.30	0.31645	0	0.04
ε/eV	0.2152	0	2.6426	0	0.0075	0.0024	0.0071	0	0.0019

Table 4 Potential functions between different atoms

Atom	Ti	Al	C	H	O
Ti	EAM	EAM	Morse	L-J	L-J
Al	EAM	EAM	Morse	L-J	L-J
C	-	-	0	L-J	L-J
H	-	-	-	L-J	L-J
O	-	-	-	-	L-J

At the same time, with the increase in scratching speed, the oscillation amplitude of F_x at steady state is obviously larger than that at low speed (50 m/s). This occurs because faster scratching speeds correlate with increased kinetic energy of the system. Elevated velocities accelerate atomic vibrations and interactions, consequently increasing the local deformation rate. When the γ-TiAl alloy atom adapts to the scratching force, it generates larger vibration, which in turn

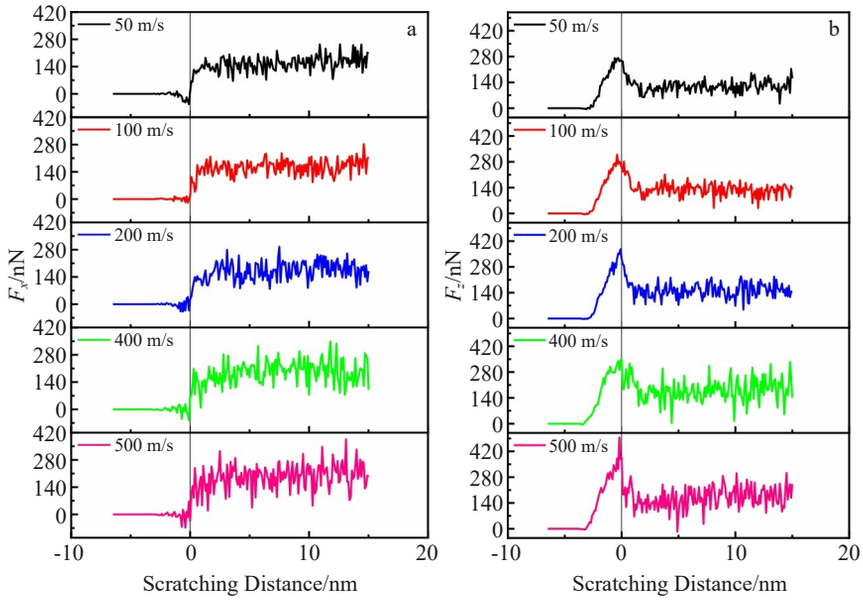


Fig.2 Variation curves of characterization forces at different speeds: (a) tangential force F_x; (b) normal force F_z

aggravates the fluctuation of F_x.

In order to more clearly express the effect of scratching speed on the scratching force, the average calculation of the force data in the stable state of 5–15 nm is carried out during scratching.

Fig. 3 shows the steady-state distribution of the scratching force at different speeds. Fig. 3a shows the distribution of the scratching force under 1-nm-thick water layer lubrication, and Fig.3b shows the distribution of the scratching force under dry scratching condition. The scratching force of the tool acting on single-crystal γ-TiAl alloy under water layer lubrication is significantly higher than that under dry scratching condition. This experimental result contradicts traditional tribological theories. The core of this anomalous outcome stems from the physical state transition of the nanoscale water layer. Relevant studies have shown that when the thickness of the water layer is of the order of several nanometers, the water layer no longer exhibits typical liquid lubrication behavior. Instead, ice-like water is formed due to the ordered hydrogen bond network[30]. The two-dimensional water layer with a thickness of several nanometers presents a quasi-solid ice-like structure[31], and its frictional behavior is highly dependent on the substrate material. In this case, when the tool passes through the water layer, it is actually scratching the interface with solid characteristics, which is similar to the scratching process under dry scratching condition.

The variation in friction coefficient reflects the variation of dominant lubrication mechanisms at different speeds: as seen in Fig.3a, under water layer lubrication, the friction coefficient first decreases and then stabilizes as the scratching speed increases. When the scratching speed is less than 200 m/s, the dominant mechanism is boundary adsorption film lubrication. Water molecules can form a complete solid-like adsorption film on the tool and workpiece surface, effectively isolating direct contact between them, so the friction coefficient increases slightly with speed. When the scratching speed is between 200 and 400 m/s, the dominant mechanism transitions to partial hydrodynamic lubrication. As the speed increases, the relative motion between the tool and the water layer intensifies. Local regions of the solid-like water film undergo transient “liquefaction” due to shear-induced heating, forming an extremely thin hydrodynamic film that further reduces the interfacial shear resistance, and the friction coefficient decreases accordingly. When the scratching speed

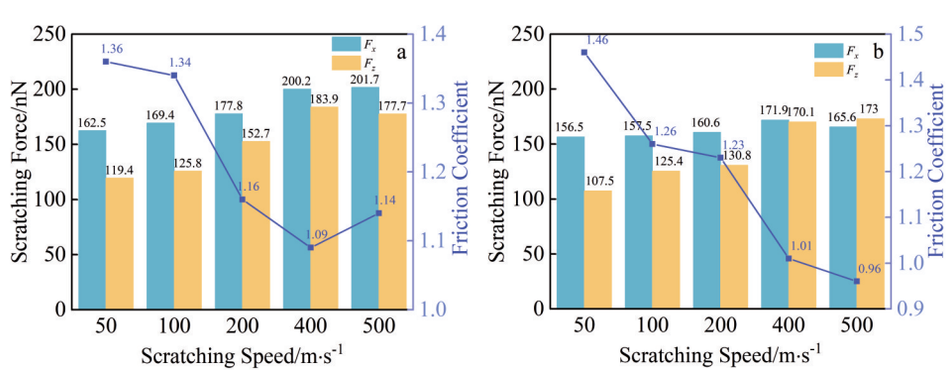


Fig.3 Scratching force and friction coefficient at different speeds under water lubrication (a) and dry scratching (b) conditions

exceeds 400 m/s, the dominant mechanism reverts to solid-like film shearing: at high speeds, the hydrodynamic film fails due to the rapid extrusion by the tool, and the water layer exists again as a solid-like adsorption film. However, at this point, the material surface undergoes slight softening due to frictional heat, which offsets part of the shear resistance and thereby keeps the friction coefficient at a low level.

As shown in Fig. 4a, as the scratching speed increases, the water layer is subjected to greater squeezing and shearing, resulting in a change in its thickness. At lower speeds, the water layer is relatively thick. As the speed increases, the water layer becomes thinner, resulting in a weakened lubrication effect. This is also verified by the number of water molecules in the groove after scratching, as shown in Fig.4b.

In contrast, the friction coefficient continues to decrease with the increase in scratching speed under dry scratching condition. This reduction stems from accelerated plastic deformation rate during high-speed scratching coupled with significant localized temperature rise, which induces material softening and consequently lowers the frictional resistance.

3.2 Effect of scratching speed on workpiece temperature

The workpiece temperature has always been regarded as an important factor in the study of nano-processing. As a macroscopic physical quantity, temperature reflects the average kinetic energy of the movement of microscopic particles.

Fig. 5 shows the change in workpiece temperature during machining. The workpiece temperature shows an upward trend with the increase in scratching distance. The temperature rise originates from the fracture of atomic bonds within the γ-TiAl

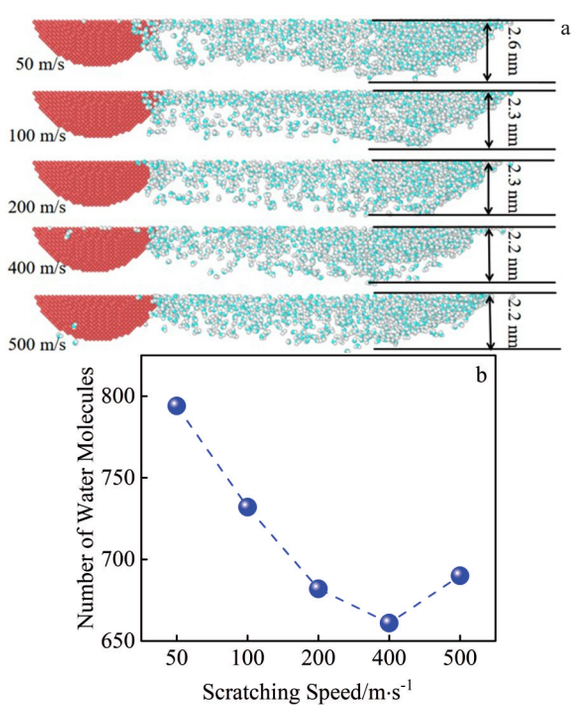


Fig.4 Distribution of water molecules in the groove along the *z*-axis (a) and number of water molecules (b) at different scratching speeds

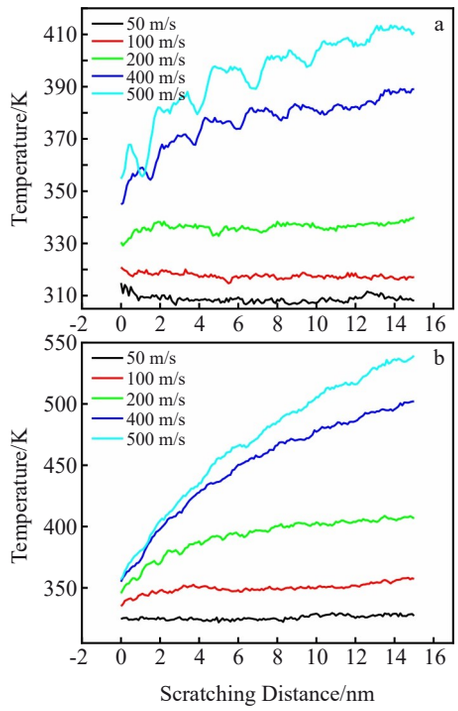


Fig.5 Temperature variation curves at different scratching speeds under water lubrication (a) and dry scratching (b) conditions

alloy workpiece during scratching, where chemical energy is converted into heat energy. However, the rate of temperature rise gradually decreases in the later period. This is because as the scratching process continues, the heat generated in the scratching area diffuses to the surrounding area through heat conduction. At the same time, the constant-temperature layer at the bottom of the γ-TiAl workpiece absorbs heat. With the advancement of the processing process, the overall temperature of the workpiece rises, and this endothermic phenomenon gradually increases. In addition, the heat dissipation of the workpiece becomes more pronounced, resulting in a slower temperature rise of the workpiece in the later stage than in the initial stage.

Fig. 5a shows the effect of scratching speed on the temperature change of the workpiece under water-layer lubrication. As the scratching speed increases, the workpiece temperature continues to rise. When the scratching speed exceeds 400 m/s, the substrate temperature of γ-TiAl workpiece shows a wavy upward trend, which can be attributed to the cooling effect of the water layer. Under the condition of water lubrication, the water layer can effectively take away the heat generated during scratching, thus slowing down the increase in the substrate temperature. The fluctuation of temperature shows that the existence of water layer greatly alleviates the temperature rise caused by friction and plastic deformation during scratching, and effectively inhibits the excessive accumulation of friction heat.

Fig. 5b shows the change trend of γ-TiAl alloy temperature during dry scratching. Compared with the water lubrication condition, the temperature rise during dry scratching is more obvious. Due to the lack of effective cooling mechanism, the

temperature rise range is large. This result further verifies the key role of the water layer in reducing the substrate temperature. Especially at high-speed scratching, the water layer can quickly take away the friction heat, thus effectively preventing the plastic deformation and wear of the workpiece surface caused by excessive temperature.

By comparing the matrix temperature distribution at different scratching speeds in Fig.6, it can be observed that the temperature around the contact point between the tool and the workpiece increases significantly. These local high-temperature regions are the key factors leading to plastic deformation of the workpiece. Excessive temperature will destroy the surface quality of the workpiece and reduce the machining accuracy. The introduction of water layer lubrication effectively reduces the formation of these high-temperature regions, thereby maintaining the surface quality and machining accuracy of the workpiece. In addition, the cooling effect of the water layer is particularly significant, which can quickly take away the heat generated during machining, thereby effectively reducing the temperature of the chip area. Compared with the dry-scratching process shown in Fig. 6b, the temperature distribution under water lubrication condition shown in Fig. 6a is significantly optimized, which not only reduces the high-temperature zone, but also reduces the thermal damage caused by excessive temperature.

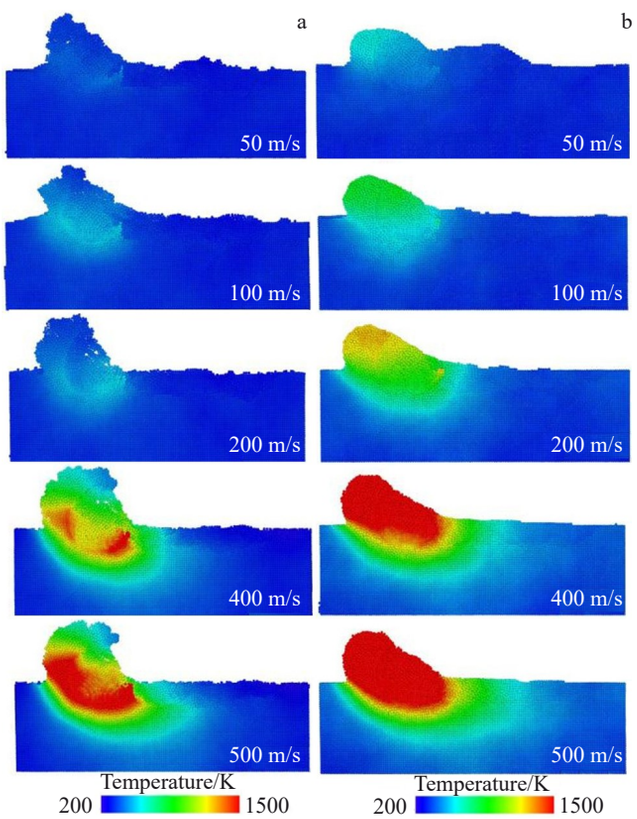


Fig.6 Temperature distribution at different scratching speeds under water lubrication (a) and dry scratching (b) conditions

3.3 Effect of scratching speed on stress distribution

From the von Mises stress distribution at different scratching speeds in Fig. 7, it can be found that as the scratching speed continues to increase, the stress concentration induced by the dynamic effect becomes more and more significant. The affected area not only shows an expanding trend on the spatial scale, but also experiences increasing local stress concentration. When the scratching speed reaches 400 m/s, the stress distribution of the matrix material becomes more uneven. Particularly, the high-stress concentration of the atoms occurs in the contact area with the rake face. During high-speed scratching, the material absorbs a large amount of mechanical energy in a short time, which promotes the obvious microstructure evolution near the contact interface (i.e., the direct contact area between the tool and the material).

3.4 Effect of scratching speed on dislocation distribution

At different scratching speeds, the generation and propagation of dislocations occur on the subsurface of single-crystal γ-TiAl alloy. Due to the high brittleness of single-crystal γ-TiAl alloy, dislocations are more likely to generate and expand on the subsurface under high stress, especially during scratching. These dislocations will expand in different directions and even lead to the formation of local slip bands. With the increase in scratching speed, the plastic deformation mechanism of the metal surface will change. The higher scratching speed means that the applied stress is larger, which promotes the plastic deformation of the crystal near the surface. In contrast, the lower scratching speed leads to a smoother deformation process, resulting in more dislocations. This occurs because lower scratching speeds prolong the

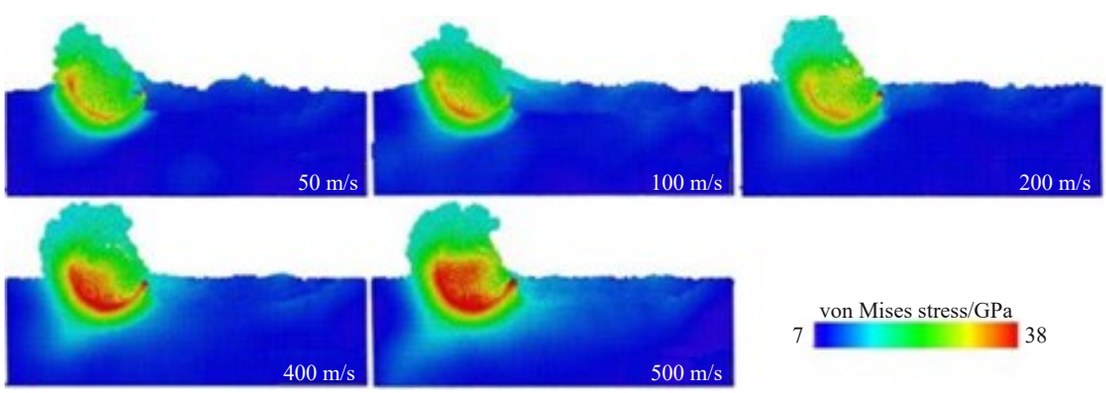


Fig.7 Stress distribution at different scratching speeds under dry scratching condition

exposure to external forces of the matrix, allowing more time for stress response and facilitating more extensive plastic deformation processes.

In the nano-processing process, the changes of the internal defects in the workpiece are shown in Fig. 8. To identify the defects in the workpiece, the common neighbor analysis (CNA) and dislocation extraction algorithm (DXA) methods are used to color different types of atoms. By this method, the perfect fcc crystal atoms are removed. In Fig. 8, white represents surface atoms and amorphous atoms, red represents hcp atoms, and two layers of red atoms represent a stacking fault structure.

Fig. 8 shows that scratching speed significantly affects chip morphology on the surface and distribution of internal defects in the matrix during nano-scratching of single-crystal γ-TiAl alloy. During scratching, the majority of the generated dislocations are partial dislocations with a Burgers vector of 1/6<112>, which are dominated by the {111} slip plane. At low scratching speeds of 50–100 m/s, these 1/6<112> partial dislocations tend to slip within the plastic deformation zone beneath the tool rake face. In this study, at high scratching speeds ranging from 200 m/s to 500 m/s, superlattice dislocations induced by the interaction between 1/6<112> partial dislocations and 1/2<110> dislocations are barely observed. Besides the predominant Shockley partial dislocations, a small number of Lomer-Cottrell dislocations are also generated. When the scratching speed is 50 m/s, a single slip plane is mainly activated inside the matrix. On this slip surface, the dislocations move and evolve in an orderly manner, forming a relatively regular chip morphology, as shown in Fig. 8a. Due to the low speed, the dislocations have enough time to fully evolve and move, so the defect area inside the matrix is small. As the scratching speed increases to 100 m/s, multiple slip planes are activated inside the matrix, as shown in Fig. 8b. The activation of these slip surfaces leads to a more complex plastic deformation process, making the formation of chips more difficult. Due to the high speed, the movement time of dislocation in the matrix is greatly shortened, resulting in more intense and disordered dislocations movement, which in turn increases the defect distribution area inside the matrix.

In order to further understand the effect of scratching speed on dislocation motion and material deformation mechanism during nano-scratching of single-crystal γ-TiAl alloy, quantitative analysis was carried out to calculate the number of dislocations in the matrix at different scratching speeds. By counting the number of dislocations at different time, the variation curves of dislocation length with scratching speed and time were drawn.

Fig. 9 shows the dislocation change curves at different scratching speeds. In the initial stage of scratching, with the application of external stress, the length of dislocation line increases rapidly, and new dislocations are continuously generated inside the material. The generation of dislocations is closely related to defects, grain boundaries, and external forces in the material lattice. As the stress continues to act on the material, dislocations continue to slip in the lattice, resulting in the aggregation or dispersion of dislocations. Therefore, the length of the dislocation line usually presents a complex fluctuation phenomenon during deformation. This fluctuation reflects the complexity and diversity of dislocation dynamics under the action of external stress and high temperature. At the same time, it also reveals the far-reaching influence of the interaction and evolution of dislocations on the mechanical properties of materials during deformation.

Fig. 9 shows that when the scratching speed exceeds 400 m/s, the length of dislocation lines is shorter than that at scratching speeds of 50, 100, and 200 m/s. A lower scratching speed leads to a lower strain rate, which slows down the movement and diffusion of dislocations in the material and reduces heat accumulation. This results in incomplete stress release in the material, thereby generating more dislocations and increasing the length of dislocation lines. This indicates that dislocations are relatively dispersed with a low density. At this point, the plastic deformation of the material is more uniform. The gradual accumulation of dislocations tends to impede subsequent slip, making the material more prone to exhibit work hardening characteristics.

At moderate-to-high scratching speeds, the increase in dislocation line length is accompanied by the activation of multiple slip systems. Enhanced dislocation interactions and localized deformation concentration may increase the work-hardening rate, but excessive dislocation entanglement may also induce local softening. Dislocations move faster under such conditions, yet the higher strain rate causes excessive localized plastic deformation. This increases dislocation density and interactions, thus generating more dislocations. High-speed movement rapidly raises the substrate temperature.

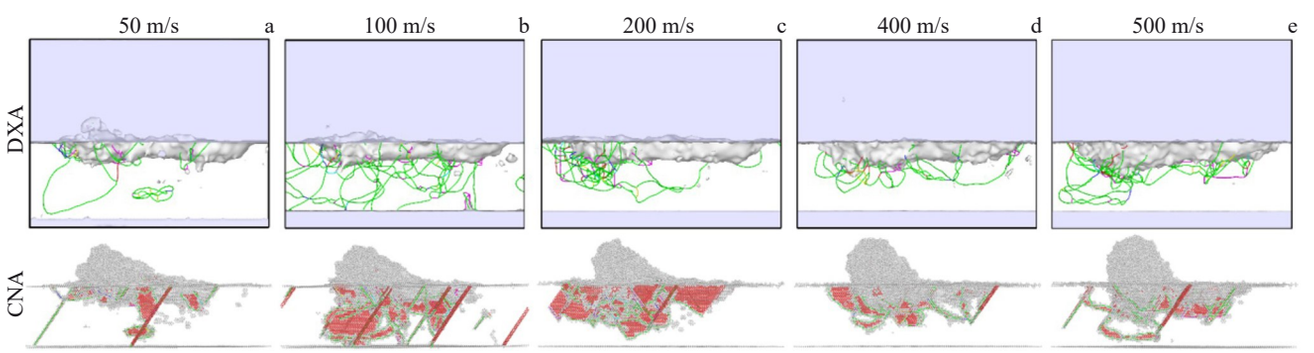


Fig. 8 Dislocation distributions at different scratching speeds

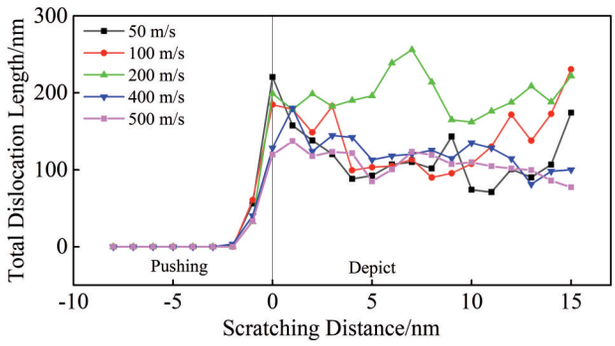


Fig.9 Dislocation change curves at different scratching speeds

Although dislocations are generated quickly, subsequent rapid cooling leads to stress concentration and dislocation aggregation, thereby increasing the length of dislocation lines.

When the scratching speed is 400 m/s, the heat-affected zone is relatively moderate, enabling effective heat dissipation and avoiding excessive heat accumulation. This ensures that dislocations can move rapidly inside the material without reaching the deformation limit. Consequently, the interactions and cross-influences between dislocations are minimal, resulting in shorter dislocation lines. At a scratching speed of 500 m/s, the length of dislocation line rebounds along with concentrated thermal stress. Dislocation aggregation tends to cause local embrittlement, leading to a decrease in material ductility. Meanwhile, rapid thermal cycling may cause competition between work hardening and thermal softening effects, ultimately resulting in a complex mechanical response.

3.5 Effect of scratching speed on surface morphology

Fig. 10 shows the distribution of chips at different scratching speeds. Fig. 10a–10e are top views, and Fig. 10a_1–10e_1 are front views. As the scratching speed increases, the volume of chip atoms accumulated at the front end of the tool gradually increases. During low-speed scratching, the chip formation and stripping are relatively slow, and the low movement speed prevents the material from acquiring enough kinetic energy to quickly break away from the tool surface. Therefore, the plastic deformation is mainly dominated by local plastic flow and shear action, which leads to heat accumulation in the characterization area. Due to heat accumulation, the heat exchange between the tool and the material is limited and cannot be effectively dissipated. As shown in Fig. 6, the local temperature of the material increases, which enhances the plasticity and promotes the formation of step-like chip morphology, as shown in Fig. 10a and Fig. 10b.

Raising the scratching speed increases the scratching force, leading to faster material removal. As shown in Fig. 10c–10e, the step phenomenon gradually disappears, and the chips are mainly accumulated on the front side of the tool. Under high-speed scratching, the rapid material flow makes it difficult to dissipate heat timely, especially at the tool-workpiece contact interface, where the temperature continues to rise. At this time, due to the plastic fluidity of the material and the high temperature in the front area of the tool, the material will soften during scratching, which further promotes rapid peeling.

During high-speed scratching, the heat accumulation interacts with the rapid flow of the material, resulting in the chip no longer staying on the material surface or forming a step-like structure, but concentrating on the front side of the tool. This phenomenon shows that the heat accumulation and mechanical behavior between the tool and the workpiece have changed significantly at a higher scratching speed, which has an effect on the morphology and distribution of the chips. From the distribution in top view of groove width at different scratching speeds in Fig. 11, it is found that the groove width also increases with increasing scratching speed. This is attributed to higher scratching force and associated plastic deformation behavior at high speed. Higher scratching speed will make the heat acting on the material accumulate rapidly. Single-crystal γ-TiAl alloy is an intermetallic compound with a high melting point and low thermal conductivity. Local

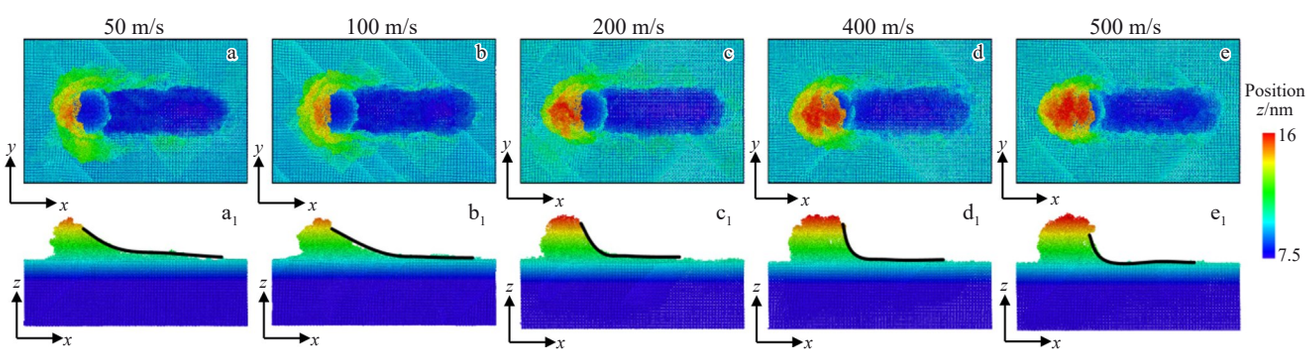


Fig.10 Distribution of chips at different scratching speeds in top view (a–e) and front view (a_1–e_1)

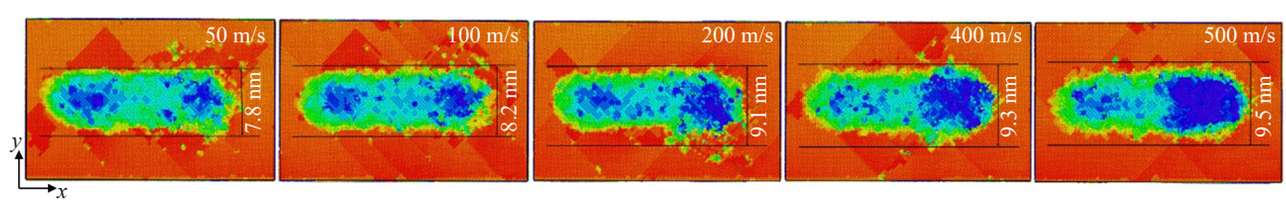


Fig.11 Distribution of groove width at different scratching speeds

softening occurs at high speeds, which reduces the material hardness and makes it easier to scratch, resulting in increased groove width. With increasing scratching speed, the local stress concentration will also expand the plastic deformation zone. The material is more prone to large-scale plastic flow at high speeds, resulting in increased scratching groove width.

Moreover, in addition to the shear effect, the geometric shape of the spherical tool also causes a significant ploughing effect. When the scratching speed is high, the rake angle of the tool and the flow characteristics of the workpiece atoms will affect the groove width. At higher scratching speed, the time for atoms to discharge from the scratching area is shortened, and the contact between the tool and the material becomes more concentrated. Therefore, due to the enhanced transverse flow of γ-TiAl alloy around the tool tip, the groove width formed by the tool also increases.

3.6 Effect of scratching speed on chips

During scratching, if the effects of workpiece atoms on the deformation and movement, as well as the effect of the tool on the workpiece atoms around the contact area, are not considered, the theoretical chip number can be obtained by volume conversion. Specifically, at the onset of the machining process, the tool initially comes into contact with the workpiece material. The atoms above the contact point are defined as an ideal set of atoms to be removed from the workpiece by the tool during scratching. These atoms are completely removed and form the chip. The theoretical number of chip atoms can be further derived by calculating the volume of this atom set. However, the actual number of chips formed is generally lower than the theoretical value, because the atoms within the contact area undergo complex deformation and flow processes under large external forces. With the advance of the tool, the atomic lattice in the contact area deforms under external force until it collapses and transforms into an amorphous state. Some amorphous atoms accumulate in front of the tool during deformation to form chips; the other part is pressed into the workpiece and becomes part of the machined surface. The chip conversion rate is defined as the ratio of actual chip atoms to theoretical chip atoms. The study of chip conversion rate is of great significance for understanding the material removal mechanism and optimizing the processing technique. The calculation results are shown in Table 5.

Fig. 12 shows the change in the number of chip atoms at different scratching speeds. With the increase in scratching speed, the number of chips of single-crystal γ-TiAl alloy shows a downward trend as a whole. However, when the scratching speed reaches 500 m/s, the number of chip atoms increases slightly. This trend is consistent with the trend of the friction coefficient at different scratching speeds in Fig.3.

At low scratching speed, the plastic deformation of single-crystal γ-TiAl alloy is mainly realized by shear and dislocation slip mechanisms, and regular chips are formed on the material surface. As the scratching speed increases, especially when it exceeds 400 m/s, the heat generated during scratching increases significantly, resulting in localized material softening. This thermal softening effect inhibits the formation of chips, so the number of chip atoms decreases with the increase in scratching speed.

At low scratching speed, more γ-TiAl alloy atoms form obvious chips due to the poor fluidity of the material. At a higher scratching speed, the material undergoes a large range of plastic flow. The thermal effect at high scratching speed leads to local softening, which reduces the hardness and facilitates scratching. This is consistent with the conclusion of Zhang et al[18] that increasing scratching speed leads to decreased material removal and increased local temperature.

Table 5 Effect of scratching speed on chip atoms

Scratching speed/mm·s^{-1}	Theoretical number of chip atoms	Actual number of chip atoms	Chip conversion rate/%
50	26355	10233	38.8
100	26355	9798	37.2
200	26355	9557	36.3
400	26355	8471	32.1
500	26355	8583	32.6

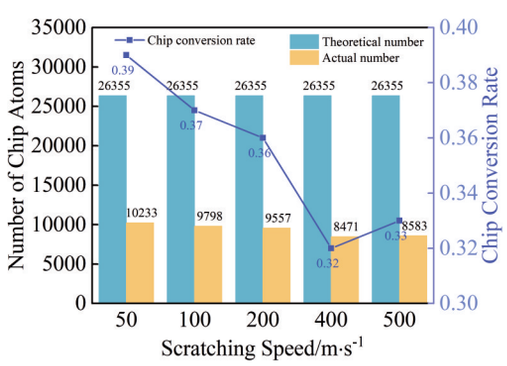


Fig.12 Effect of scratching speed on the number of chip atoms and chip conversion rate

3.7 Effect of scratching speed on surface roughness

Machining speed directly affects the surface roughness. Specifically, scratching speed has a direct and significant impact on the micro-morphology and roughness of the final workpiece surface. There are many methods to evaluate the roughness of diamond mechanical grinding. In practice, the most commonly used parameters are arithmetic average height and root mean square height, with their characterization formulas shown in Eq. (6–7):

$$S_a = \frac{1}{MN}\sum_{i=0}^{M}\sum_{j=0}^{N}\left|z\left(x_i, y_j\right)\right| \quad (6)$$

$$S_q = \sqrt{\frac{1}{MN}\sum_{i=0}^{M}\sum_{j=0}^{N} z^2(x_i, y_j)} \quad (7)$$

where, S_a is the arithmetic mean height of the three-dimensional contour; S_q is the root mean square height; N is the number of row sampling points; M is the number of column sampling points; $z(x_i, y_j)$ is the height of the sampling point in the jth column of the ith row.

Fig. 13 shows the surface roughness value calculated by Eq. (6) and Eq. (7) after extracting the discrete atoms of the machined surface at different scratching speeds.

Fig. 13 shows the surface roughness data at different scratching speeds and the surface topography after processing under water lubrication. As depicted in Fig. 13a, workpiece surface roughness decreases significantly with increasing scratching speed. This trend is attributed to rapid frictional heating at the tool-workpiece interface, which thermally softens the material locally and enhances its plastic deformation capacity. Under water lubrication, water not only has a cooling effect and reduces the thermal damage, but also reduces the friction coefficient between the tool and workpiece through the lubrication effect. This reduces the friction resistance and heat generations, thereby limiting the plastic deformation and micro-damage of the surface, and finally achieving low surface roughness. This is consistent with the conclusion of Ou et al[32] that lubrication can significantly improve the surface quality.

Compared with the surface roughness under dry scratching conditions, the surface roughness under water lubrication is obviously lower. During dry scratching, the lack of effective cooling and lubrication leads to elevated temperature and increased friction force, which tend to cause obvious scratches and irregular surface structures on the workpiece. These factors lead to a significant increase in surface roughness. In conclusion, an appropriate scratching speed (e. g., 400 m/s) effectively balances heat accumulation and dissipation, reduces dislocation line length, and optimizes the deformation behavior of the material.

3.8 Experimental results of TiAl alloy at different scratching speeds

In this research, the Keysight G200 nano-indentation instrument was used for nano-scratching experiments. The equipment is equipped with a high-precision scanning probe microscope, which can perform high-resolution three-dimensional scanning imaging on the surface of the processed workpiece to obtain detailed information. After the scratching experiment, the three-dimensional morphology of the metal scratches was observed using a ZeGage Pro 3D optical surface measuring instrument. It is worth noting that the MD simulation adopted in this research differs from the nano-scratching experiment in terms of research methods. The two parts of the study have distinct independence in terms of scale, but they can be complementary from the perspectives of microscopic mechanisms and macroscopic phenomena[33].

In this nano-scratching experiment of TiAl alloy, the surface of the Ti-48Al-2Cr-2Nb alloy specimen with a fully lamellar microstructure was first ground step-by-step using 400#, 800#, 1500#, and 2000# SiC sandpapers in sequence. Subsequently, mirror polishing was performed on a polisher using diamond pastes with grit sizes of W1.5 and W0.5. Finally, the specimen was ultrasonically cleaned in acetone and ethanol for 10 min each to completely remove surface contaminants, and then blow-dried with high-purity nitrogen for subsequent use. In the nano-scratching experiment, the scratching speed was 2000, 4000, and 6000 μm/min, the normal scratching load was 20 N, and the scratching distance was 1000 μm. An atomization method was employed to precisely provide a thin and uniform water film on the cutting area of the sample. This experiment has strict requirements on environmental conditions to ensure the accuracy and repeatability of the experimental results. Therefore, during the experiment, the laboratory temperature and humidity were

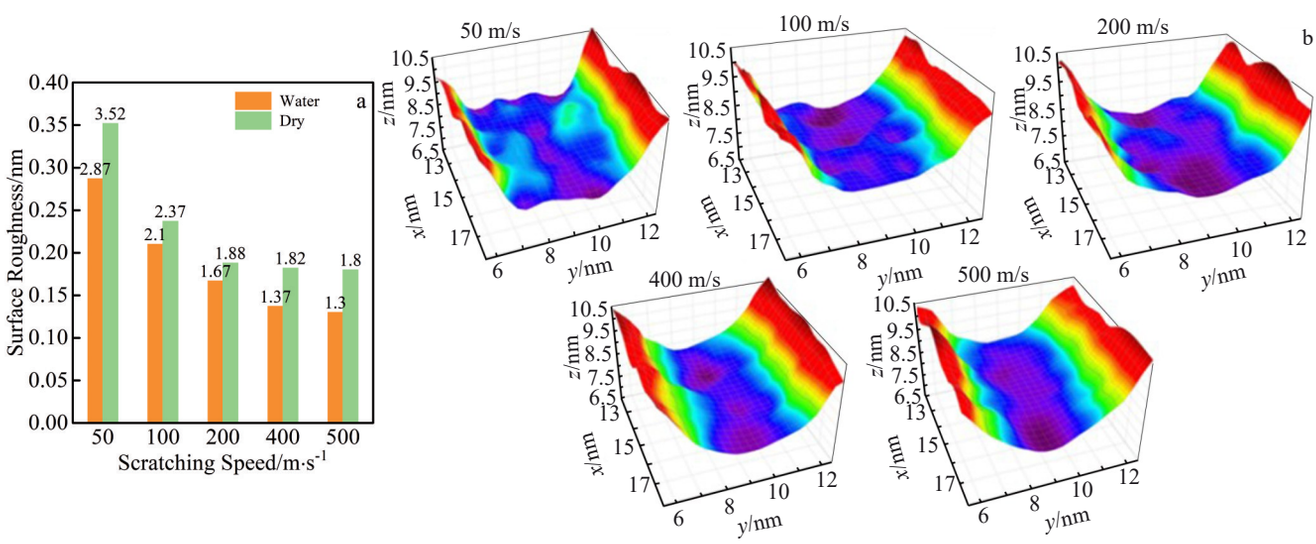


Fig.13 Surface roughness at different speeds with and without water lubrication (a); machined surface topographies at different scratching speeds after processing under water lubrication (b)

strictly controlled at 23±5 ℃ and 40%±5%, respectively. In addition, in order to reduce the interference of external factors on the experiment, vibration around the experimental setup should be minimized to avoid compromising equipment accuracy and measurement results, ensuring experimental stability and data reliability. Based on the above specific experimental parameters, three sets of nano-scratching experiments of TiAl alloy under different conditions were designed, as shown in Table 6.

Fig. 14 presents the grayscale morphological images and color height cloud maps of the scratch surfaces at different scratching speeds. Fig. 14 shows that when the scratching speed is 2000 μm/min, the defects on the surface of TiAl workpiece have a significant effect on the scratching process. At this speed, the surface micro-defects (such as micro-cracks, pores, or uneven hardness, etc.) interfere with the scratching process, resulting in a slight shift in the scratching morphology. The defect region leads to increased scratching resistance or decreased plastic deformation performance of the local material, thus affecting the stability of the scratching path. This phenomenon deteriorates the surface quality around the scratch, where irregular material flow promotes roughness development and causes uneven surface morphology on both sides, with pronounced ripples and localized accumulation. With the increase in scratching speed, the change of scratching width remains relatively stable, and there is no significant fluctuation. However, Fig. 15 shows that the flow distribution on both sides gradually becomes uniform. This

Table 6 Nano-scratching experiments of TiAl alloy under different parameters

Scratching speed, v/μm·min^{-1}	Normal load, F_z /N
2000	20
4000	20
6000	20

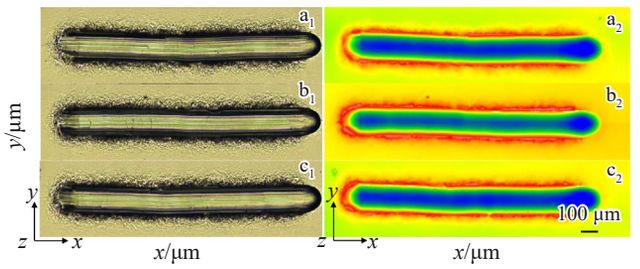


Fig.14 Grayscale morphology images ($a_1 - c_1$) and colored height cloud maps (a_2–c_2) of scratched surfaces at different scratching speeds: ($a_1 - a_2$) 2000 μm/min; ($b_1 - b_2$) 4000 μm/min; (c_1–c_2) 6000 μm/min

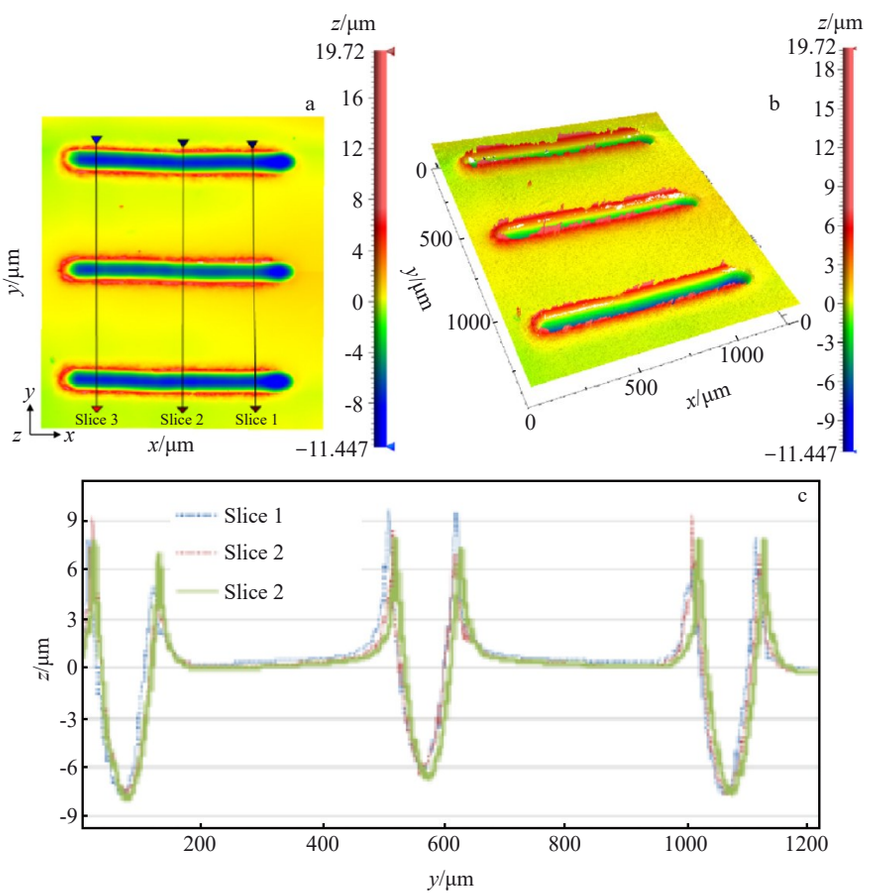


Fig.15 Scratch optical topographies at different scratching speeds: (a) 2D false-color height contour map; (b) 3D rendered surface topographies; (c) 2D cross-section profiles extracted from the positions marked in Fig.15a

phenomenon shows that the chip deformation in the scratching area tends to be balanced at a higher scratching speed, and the stress distribution during scratching gradually becomes uniform.

This indicates that higher scratching speed (e. g., 6000 μm/min) promotes a faster scratching process and reduces the influence of heat input and local plastic deformation on the material. Consequently, material flow becomes more uniform, minimizing excessive softening or plastic flow caused by local temperature rise. Therefore, the lateral flow on both sides of the scratch becomes more regular and symmetrical. This stabilization of material flow ultimately improves the surface quality of the specimen.

In general, MD simulation is mainly used to study the mechanism of the nano-scale scratching process, and its simulation scale is significantly different from that of actual machining conditions. Therefore, MD method is mainly used as a theoretical analysis tool at present, and the direct migration to practical engineering applications still faces challenges. Future research should focus on integrating the micro-deformation mechanism revealed at nano-scale into the macro-cutting simulation framework to construct cross-scale prediction models. At the same time, the calibration and verification of simulation parameters through high-precision experimental data can realize the deep fusion of theoretical mechanism and experimental observation, thus significantly enhancing the prediction reliability, universality, and engineering guidance value of the model.

4 Conclusions

1) Increasing scratching speed significantly elevates scratching forces and promotes frictional heat generation. Higher scratching speeds lead to localized temperature rise and stress concentration in the γ-TiAl alloy. Compared to dry scratching condition, water lubrication effectively reduces the friction coefficient, facilitates heat removal, minimizes thermal damage, and consequently enhances surface quality and machining precision.

2) At the microstructural level, variations in scratching speed significantly influence dislocation motion and defect distribution within the material. Higher scratching speeds induce more intense dislocation motion and defect proliferation, and promote chip accumulation on the tool rake face, affecting chip formation and distribution. An appropriate scratching speed (e. g., 400 m/s) effectively balances heat accumulation and dissipation, reduces dislocation line length, and optimizes the deformation behavior of the material.

3) The surface roughness of the machined surface decreases significantly with increasing scratching speed. This reduction is particularly pronounced under water lubrication, where cooling and lubrication further lower surface roughness. Water lubrication reduces surface plastic deformation and micro-damage, enabling the maintenance of lower surface roughness. Generally, scratching speed and water lubrication conditions collectively determine the machining performance and surface quality of single-crystal γ-TiAl alloy. Optimizing both scratching speed and water lubrication conditions is crucial for enhancing machining efficiency and surface quality.

4) Experimental validation confirms that scratching speed significantly affects surface quality. Lower scratching speeds (e. g., 2000 μm/min) are prone to interference from surface micro-defects on the specimen, leading to irregular scratch morphology and increased surface roughness. Conversely, higher scratching speeds (e.g., 6000 μm/min) reduce localized heat input and plastic deformation, promote more uniform material flow, and result in smoother scratch morphology. The results demonstrate that appropriately increasing the scratching speed helps to optimize the distribution of scratching forces and improves machining precision.

References

1 Zhao J C, Westbrook J H. *MRS Bulletin*[J], 2003, 28(9): 622

2 Ezugwu E, Wang Z. *Journal of Materials Processing Technology*[J], 1997, 68(3): 262

3 Wang H, Subhash G. *Journal of the Mechanics and Physics of Solids*[J], 2002, 50(6): 1269

4 Wang Y C, Shi J. *Nanoscale Research Letters*[J], 2013, 8: 389

5 Ishii N, Tanaka R, Kojima Y *et al. Key Engineering Materials*[J], 2015, 656: 296

6 Zhao W, Ren F, Iqbal A *et al. The International Journal of Advanced Manufacturing Technology*[J], 2020, 106: 1497

7 Tang C, Zhang L. *Nanotechnology*[J], 2004, 16(1): 15

8 Zhou P, Li J, Wang Z *et al. Ceramics International*[J], 2020, 46(16): 24961

9 Shi J Q, Fang L, Sun K *et al. Friction*[J], 2020, 8: 323

10 Sharma M, Chen C C A, Gupta A. *ECS Journal of Solid State Science and Technology*[J], 2021, 10(5): 054001

11 Tian Y, Feng H, Li J *et al. Applied Surface Science*[J], 2021, 545: 148957

12 Zhou Y, Huang Y, Li J *et al. Tribology International*[J], 2022, 175: 107802

13 Zhou Y, Huang Y, Li J *et al. Diamond and Related Materials*[J], 2023, 133: 109710

14 Wang W, Hua D, Zhou Q *et al. Applied Surface Science*[J], 2023, 616: 156490

15 Shikimaka O, Prisacaru A. *Materials Research Express*[J], 2019, 6(8): 085011

16 Zhu J, Xiong C, Ma L *et al. Tribology International*[J], 2020, 150: 106385

17 Li J, Liu B, Luo H *et al. Computational Materials Science*[J], 2016, 118: 66

18 Zhang J, Sun T, Yan Y *et al. Materials Science and Engineering A*[J], 2009, 505(1–2): 65

19 Wang B, Liu Z, Su G *et al. International Journal of Mechanical Sciences*[J], 2015, 104: 44

20 Su G, Liu Z, Li L *et al. International Journal of Machine Tools and Manufacture*[J], 2015, 89: 202

21 Shimada S, Ikawa N. *CIRP Annals*[J], 1994, 43: 51

22 Albano A, le Guillou E, Danzé A *et al. Chem Engineering*[J], 2021, 5(2): 30
23 Stukowski A. *Modelling and Simulation in Materials Science and Engineering*[J], 2009, 18: 015012
24 Li H Y, Qiao H Y, Feng R C *et al. Rare Metal Materials and Engineering*[J], 2020, 49(6): 1931
25 Zope R R, Mishin Y. *Physical Review B*[J], 2003, 68(2): 024102
26 Pei Q, Jhon M H, Quek S *et al. Computational Materials Science*[J], 2021, 188: 110239
27 Li J, Qiao H, Lei C *et al. Metals*[J], 2019, 9(12): 1278
28 Gong H, Lu W, Wang L *et al. Computational Materials Science*[J], 2012, 65: 230
29 Horn H W, Swope W C, Pitera J W *et al. The Journal of Chemical Physics*[J], 2004, 120(20): 9665
30 Gao T, Wang G, Chen X *et al. Acta Mechanica Solida Sinica*[J], 2025, 38(2): 183
31 Wu D, Zhao Z, Lin B *et al. Science*[J], 2024, 384(6701): 1254
32 Ou Z, Wu W, Dai H. *Tribology International*[J], 2023, 180: 108267
33 Liu B, Jiang K, Chen Y *et al. Nanotechnology and Precision Engineering*[J], 2025, 8(1): 68

水润滑下刻划速度对γ-TiAl合金纳米刻划性能的影响

周宝成[1,2]，黄倩倩[1]，刘世伟[1]，曹　卉[1,3]，芮执元[1,3]，冯瑞成[1,3]
(1. 兰州理工大学 机电工程学院，甘肃 兰州 730050)
(2. 重庆交通大学 绿色航空技术研究院，重庆 401135)
(3. 兰州理工大学 有色冶金新装备教育部工程研究中心，甘肃 兰州 730050)

摘　要：γ-TiAl合金具有优异高温轻质特性，但其本征脆性导致精密加工困难。水润滑可降温并缓解摩擦热积聚、刀具磨损及裂纹问题，是极具前景的加工γ-TiAl合金手段。探索了水润滑下单晶γ-TiAl合金纳米刻划速度对材料刻划力、温度变化、塑性变形和表面质量的影响。结果表明，刻划速度与水润滑共同决定单晶γ-TiAl合金的加工性能与表面质量。划擦速度增大会显著提升划擦力与摩擦热，导致局部升温与应力集中。然而，在水润滑条件下，当水层厚度为1 nm时，基底温度波动较小，具有良好的冷却效果。刻划速度为400 m/s时，水润滑能减轻表面塑性变形与损伤，切屑堆积增多，表面粗糙度降低。实验结果同样说明，刻划速度对表面质量存在显著影响。

关键词：γ-TiAl合金；纳米刻划；刻划速度；水润滑；表面质量

作者简介：周宝成，男，1985年生，博士生，重庆交通大学绿色航空技术研究院，重庆 401135，E-mail：woxinyijiu.870116@163.com